ORGANIC CHEMISTRY FRONTIERS

RESEARCH ARTICLE

View Article Online
View Journal | View Issue

Cite this: *Org. Chem. Front.*, 2022, **9**, 2343

Metal ion determined self-assembly using terpyridine building blocks†

Qixia Bai,‡[a] Ying Liu,‡[a] Tun Wu,*[a] Haoyue Su,[c] Gang Chen,[a] Yuming Guan,[a] Ming Wang,[c] Ting-Zheng Xie,[a] Zhe Zhang*[a,b] and Pingshan Wang *[a]

Received 29th January 2022,
Accepted 7th March 2022

DOI: 10.1039/d2qo00102k

rsc.li/frontiers-organic

Due to the dynamic reversibility of the coordination-driven force, the structures of metallocages are sensitive to many stimuli, including ligand geometry, temperature, concentration, anions, pH, light, and so on. Among these, the strength of the metal–ligand dative bonds is distinctly important; however, it has largely been ignored. In this contribution, a novel metal–organic ligand **L** was synthesized. On coordinating with transition metals possessing distinct binding abilities like Zn(II), Co(II), and Cd(II), diverse three-dimensional metal–organic supramolecular structures could be generated. To sum up, using metal ions with a strong ligand binding ability (Co, Zn) favors the development of larger structures [M_8L_4], whereas metal ions with a weak ligand binding ability (Cd) lead to smaller structures [M_6L_3].

Introduction

Fabricating sophisticated discrete supramolecular structures, particularly three-dimensional supramolecular cages, from simple molecular building blocks has attracted extensive attention.[1,2] It is not only because of their intriguing structures, but also owing to their diverse applications in molecular recognition,[3] sensing,[4,5] and supramolecular catalysis.[6] Along with the interest in self-assembly processes, the transition of two structures has received a significant attention.[7,8] Owing to the dynamic and reversible nature of the coordination-driven force, the structure of metal supramolecular self-assembly is mostly determined by two major elements: (i) the nature of the building blocks,[9] such as metal ions[10] and ligands,[11] and (ii) extrinsic factors such as concentration,[12,13] solvents,[14] anions,[15,16] and light,[17] among others.[18] Ligands and metal ions are undoubtedly the most important building blocks in terms of design. Metals usually serve as the polyhedron's vertex, with ligands constituting the polyhedral cage's edge.[19,20] Nitschke reported metal ion and anion determined supramolecular transformations in 2014.[21] However, in such systems, multiple factors were affected and only a limited number of metal ions were used. Either due to the shortage of the metals accessible for ligand coordination or due to the characterization difficulties, the effect of varied metal–ligand binding abilities on the self-assembly of metallostructures has rarely been described. A comprehensive understanding of the influencing factors is vital to attain precise control over the self-assembly process and achieve specific practical applications.

2,2′:6′,2″-Terpyridines are widely used as tridentate ligands due to their ability to coordinate with various transition metals,[22,23] and the binding ability with different metal ions increases in the order of Mn < Cu < Cd < Zn < Co.[24] This unique characteristic supports the primacy of the terpyridyl ligand in enhancing the complexity of complexes. Inspired by this fact, it was aimed to investigate the influence of using metals with different binding capacities on the structure of metal–organic supramolecular cages. In-depth research on this aspect can help us to effectively understand the self-assembly process, as well as provide a new technique for enhancing the supramolecular diversity, thus inspiring the construction of various adaptive or stimuli-responsive materials.

We have previously described the assembly of a series of two-dimensional clover leaf-shaped supramolecules using a tetrakis-terpyridine ligand possessing the same angle as various transition metal ligands.[25] Based on this study, a novel tetratopic metal–organic ligand **L** was synthesized using dibromobenzofuran to link with an "X" shaped tetrakis-terpyridine ligand *via* ⟨tpy-Ru^{2+}-tpy⟩ connectivity (Scheme S1†). Subsequently, as ligand **L** was self-assembled with metals possessing a strong binding ability (Co, Zn), it afforded the tetra-

[a]*Institute of Environmental Research at Greater Bay Area; Key Laboratory for Water Quality and Conservation of the Pearl River Delta, Ministry of Education; Guangzhou Key Laboratory for Clean Energy and Materials; Guangzhou University, Guangzhou 510006, China. E-mail: chemwps@csu.edu.cn, zhezhang2018@gzhu.edu.cn, chemwt@gzhu.edu.cn*

[b]*Guangdong Provincial Key Laboratory of Functional Supramolecular Coordination Materials and Applications, Jinan University, Guangzhou 510632, China*

[c]*State Key Laboratory of Supramolecular Structure and Materials, College of Chemistry, Jilin University, Changchun, Jilin 130012, China*

†Electronic supplementary information (ESI) available. See DOI: 10.1039/d2qo00102k

‡These co-first authors contributed equally.

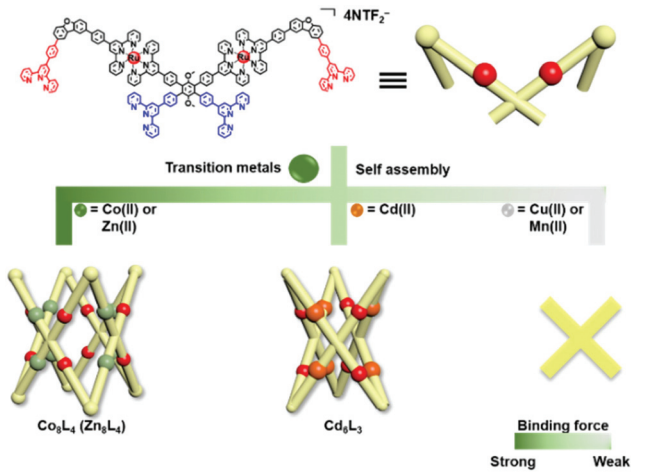

Scheme 1 Self-assembly of Zn_8L_4, Co_8L_4, and Cd_6L_3 obtained through the coordination of L with Zn^{2+}, Co_2^{+}, and Cd^{2+}.

meric cages [Co_8L_4] and [Zn_8L_4], whereas a trimeric cage [Cd_6L_3] was obtained in the case of Cd^{2+} (weak binding ability with tpy) (Scheme 1). In terms of more labile Mn and Cu, simple oligomers could be derived. As a result, the generation of metallocages can be controlled by the binding ability of the metal–organic dative bonds. Furthermore, the introduction of different metal ions is expected to facilitate a study on metal-dependent redox reactions such as the oxygen evolution reaction (OER).

Results and discussion

Synthesis and characterization of Zn_8L_4 and Co_8L_4

The key ligand **L** was obtained by a 4-fold Suzuki coupling reaction of precursor **7** with 4-(2,2′:6′,2″-terpyridyl)-phenylboronic acid (Fig. 1a). Subsequently, the ligand **L** was assembled with $Zn(NTf_2)_2$ in an exact stoichiometric ratio of 1 : 2. After heating the mixture at 60 °C for 8 h, a saturated solution of $LiNTf_2$ in methanol was added, and the resulting red precipitate was washed multiple times with methanol and water. The final solid Zn_8L_4 was obtained after drying *in vacuo* with a yield of 98%. Similarly, self-assembly with other metals was performed using $CoCl_2{\cdot}6H_2O$.

Firstly, as observed in Fig. 2a, four sets of single peaks appear at 9.11, 9.02, 8.87, and 8.80 ppm, attributed to the four different sets of tpy-$H^{3',5'}$ protons for ligand **L**, A–D, respectively. The peaks of 6,6″ protons in the uncoordinated tpy units in **L** (tpy-C, D) exhibit a dramatic upfield shift from 8.78 and 8.76 ppm to 7.48 ppm (Fig. 2a, $\Delta\delta$ = 1.33 ppm), owing to the electron shielding effect. Meanwhile, as compared with the signals of the free tpy group of **L**, those of the protons attributed to C-tpy$H^{3',5'}$ and D-tpy$H^{3',5'}$ shifted downfield, from 8.87 and 8.80 ppm to 9.12 ppm. The whole proton assignments of ligands and Zn_8L_4 were confirmed by 2D COSY and NEOSY NMR (Fig. S22–S26†). Moreover, the narrow bands at $\log D$ = −9.85 in the DOSY spectrum unambiguously reveal the presence of a single discrete species in CD_3CN (Fig. 2b). The diffusion coefficient D has been calculated to be 1.41×10^{-10}. Based on the Stokes–Einstein equation, the diameter of Zn_8L_4 is 4.22 nm, which is consistent with the model data (4.18 nm). As is well known, Co(II) exhibits stronger paramagnetic properties, which make it difficult to characterize the Co(II) complexes by ^{1}H NMR; thus, a satisfactory result has not been obtained.[26,27]

Furthermore, the ESI-MS experiments supported the formation of supramolecular structures. Fig. 2c depicts a series of continuous charge peaks from 10+ to 24+, which is attributed to the continuous loss of the anion. It is observed to be in perfect agreement with the values obtained from the simulations, and the calculated molecular weight of 22 029 Da corresponds to the molecular mass of the tetramer [$(C_{200}H_{130}N_{24}O_4)_4Ru_8Zn_8(NTf_2^-)_{32}$]. The experimentally deter-

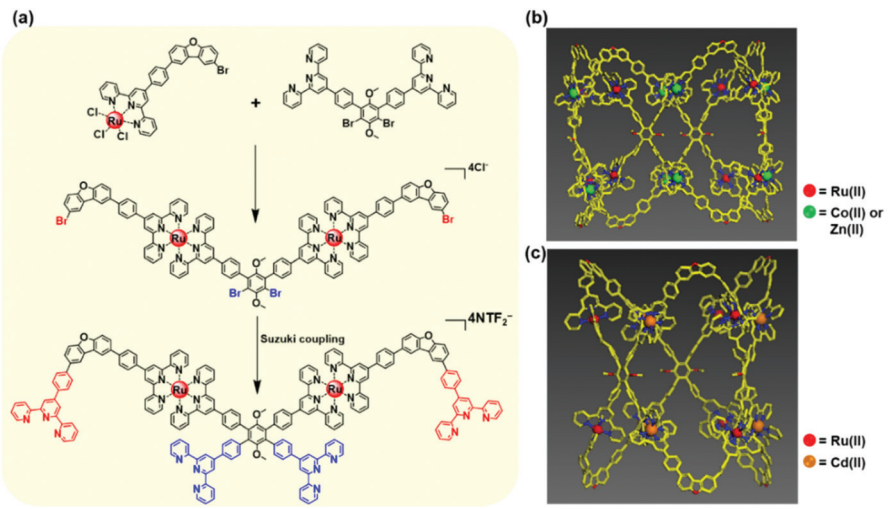

Fig. 1 (a) Synthesis of ligand **L**, (b) representative energy-minimized structure of Co_8L_4 (Zn_8L_4), and (c) representative energy-minimized structure of Cd_6L_3.

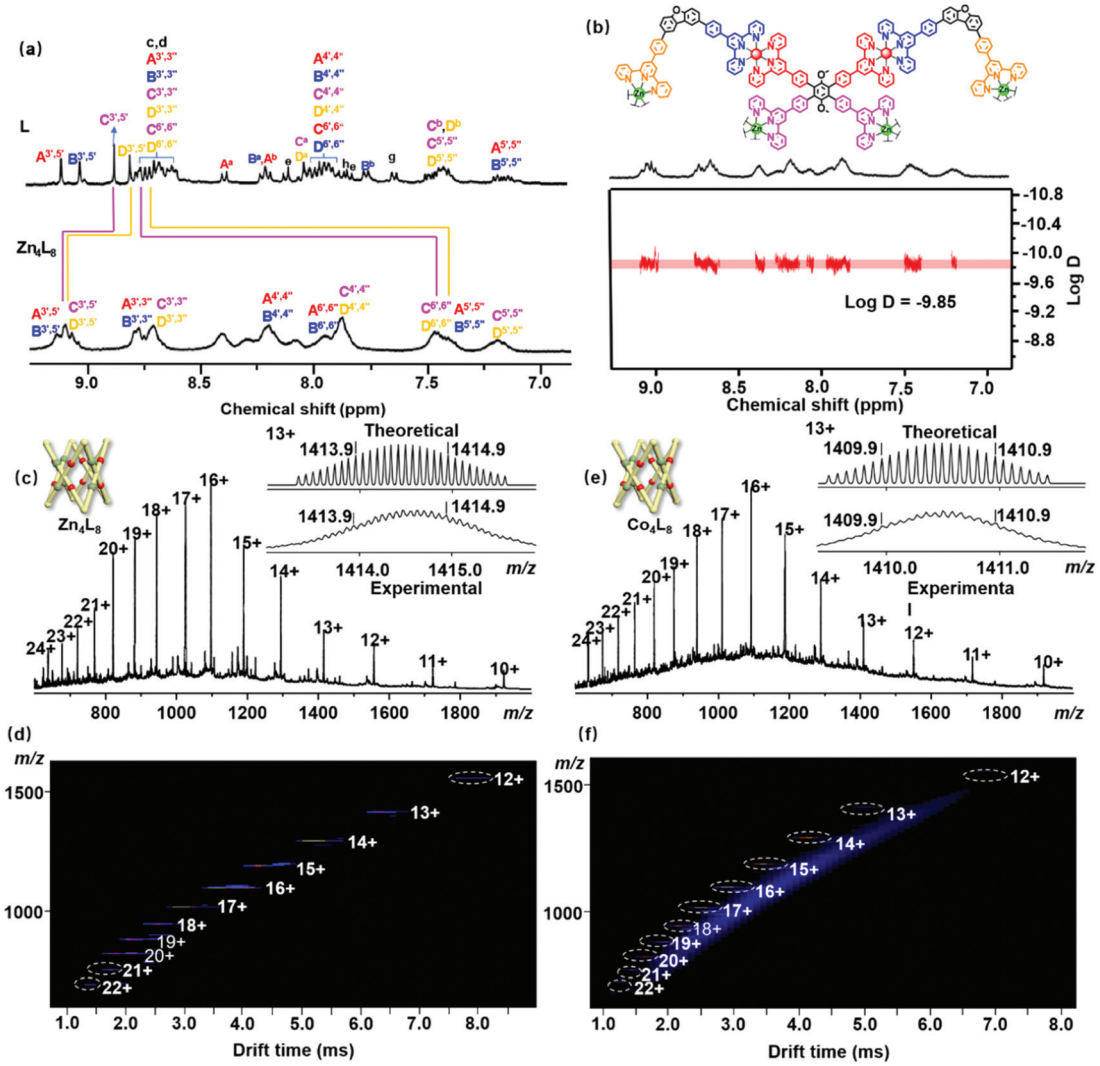

Fig. 2 (a) ^{1}H NMR of ligand **L** and $\mathbf{Zn_8L_4}$ (500 MHz, CD_3CN, 300 K), (b) 2D DOSY of $\mathbf{Zn_8L_4}$ (500 MHz, CD_3CN, 300 K), (c) and (d) ESI-MS of and TWIM-MS plots of $\mathbf{Zn_8L_4}$, and (e) and (f) ESI-MS of and TWIM-MS plots of $\mathbf{Co_8L_4}$.

mined isotope patterns for each charge state match well with the corresponding theoretical distribution (Fig. S7†). Subsequently, traveling wave ion mobility mass (TWIM)[28] spectrometry experiments were employed to distinguish the presence of isomers and provide structural information. A narrow series of drift time spectra from 12+ to 22+ can be observed in Fig. 2d, and the ESI-MS data indicated no other isomers and conformers. Moreover, the molecular weights of $\mathbf{Co_8L_4}$ are confirmed to correspond to their proposed molecular compositions (Fig. 2e), and the complexes with Co(II) have comparable drift times in the same charge states (Fig. 2f), thus indicating similar shapes of the complexes.

Synthesis and characterization of $\mathbf{Cd_6L_3}$

The previous investigations have shown that the different transition metals exhibit varying binding abilities to terpyridine. Hence, it is assumed that a distinct structure will be generated on carrying out the assembly with Cd. As illustrated in Fig. 3a, the NMR spectrum of $\mathbf{Cd_6L_3}$ is entirely different from the former; however, the spectrum of the obtained supramolecular structure exhibits a broad peak in the aromatic region compared to that of the ligand **L**. It may be caused by the slow motion of the large structure on the NMR timescale. The signals assigned to the 6,6″-tpy protons of the free tpy units are noted to exhibit a distinct upfield shift from 8.78 and 8.80 ppm to 7.50 ppm ($\Delta\delta$ = 1.28 ppm) after coordination with Cd(II). Similar to the DOSY spectrum of $\mathbf{Zn_8L_4}$, the formation of a single component in CD_3CN can be confirmed from the diffusion coefficient $\log D = -9.70$ m^2 s^{-1} for all relevant peaks (Fig. 3b). In addition, the ESI-MS analysis reveals a new set of dominant peaks ranging from 8+ to 18+ ions, thus confirming the composition of the generated structure consisting of six Cd^{2+} ions and three ligands **L** (Fig. 3c). The isotopic pattern of each charge state is consistent with the corresponding simulated values (Fig. S8†). In addition, in the 2D TWIM-MS plot, all charge states are found in a narrow band, indicating a

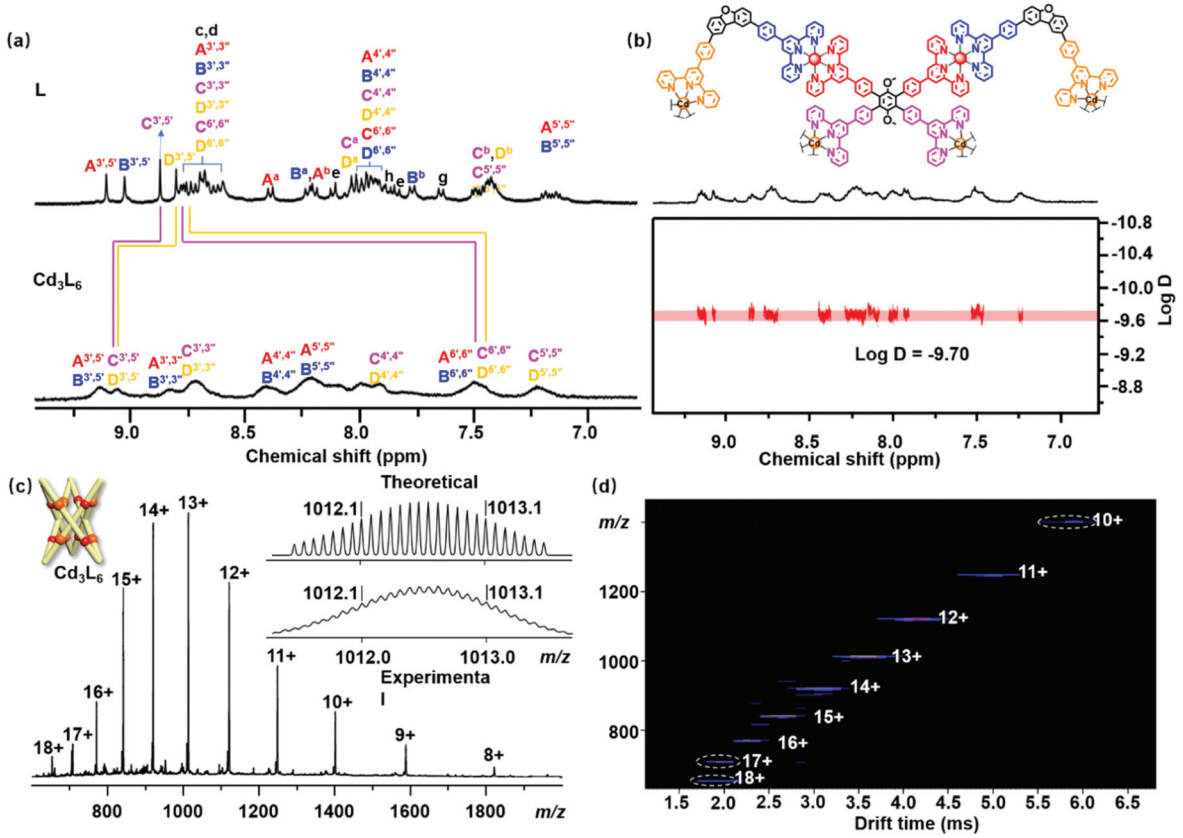

Fig. 3 (a) ^{1}H NMR of ligand **L** and $\mathbf{Cd_6L_3}$ (500 MHz, CD_3CN, 300 K), (b) 2D DOSY of $\mathbf{Zn_8L_4}$ (500 MHz, CD_3CN, 300 K), and (c) and (d) ESI-MS of and TWIM-MS plots of $\mathbf{Cd_6L_3}$.

single component with high conformational rigidity (Fig. 3d). Furthermore, as the assembly is performed using Cu and Mn, only simple oligomeric structures are obtained, most likely due to the weak binding ability to the tpy units.[29]

To further investigate the strength of the binding ability of the three metals, the stability of the three supramolecular structures was examined by gradually enhancing the collision energy using gradient tandem mass spectrometry.[30] No obvious fragments of 13+ ion for $\mathbf{Co_8L_4}$ can be detected below 20 V. As the voltage is increased to 28 V, the fragmentation peak starts to appear, and the ion peak is completely dissociated by 36 V. $\mathbf{Zn_8L_4}$ and $\mathbf{Cd_6L_3}$ have also been measured under the same conditions, with the former completely splitting at 30 V, while the latter becoming fragmented at 23 V (Fig. S9†). These results further demonstrate that the binding capability of Cd ions is substantially lower than that of Zn and Co ions, implying that the stability of the supramolecular structures formed will be inferior.[31] It is concluded that entropy plays a critical role during the process of molecular change. For metal ions with a weak binding ability, it is difficult to support the larger structures when coordinated with ligands, which tends to form small structures with more molecules in the system for achieving an entropy increase. In contrast, for metal ions with a strong binding ability, there exist sufficient binding forces to support the formation of larger structures.[13,32]

Size characterization by transmission electron microscopy (TEM) and atomic force microscopy (AFM)

To provide additional structural evidence, TEM and AFM analyses were performed on ultrathin carbon film-coated Cu grids or newly cleaved mica flakes by placing drops of dilute solutions of the three supramolecular structures dissolved in CH_3CN at a concentration of 10^{-6} M. As shown in Fig. 4e–j, the TEM images reveal several homogeneous dots with a diameter of 6.5 nm in the case of $\mathbf{Zn_8L_4}$ and $\mathbf{Co_8L_4}$ and 4.1 nm for $\mathbf{Cd_6L_3}$ (Fig. S32†), which are substantially similar to the sizes simulated using the molecular model (Fig. 4a–d). Similarly, the AFM images demonstrated a series of dots with an average height of 4.2 and 4.4 nm (Fig. 4o–q), according to the height statistical histogram of AFM for 100 particles (Fig. 4l–n), which is consistent with the calculated heights of 4.0 and 4.1 nm for the model structures of $\mathbf{Zn_8L_4}$ ($\mathbf{Co_8L_4}$) and $\mathbf{Cd_6L_3}$ structures. Due to the unavoidable tip broadening effect, the measured width of the dots in the AFM image displays large values in the 2D AFM images (Fig. S33†).[33]

CV and photophysical properties of supramolecular structures

Finally, the electrochemical properties of these fractals were investigated in a three-electrode electrochemical cell, which is composed of a 3 mm glassy carbon working electrode (WE), a

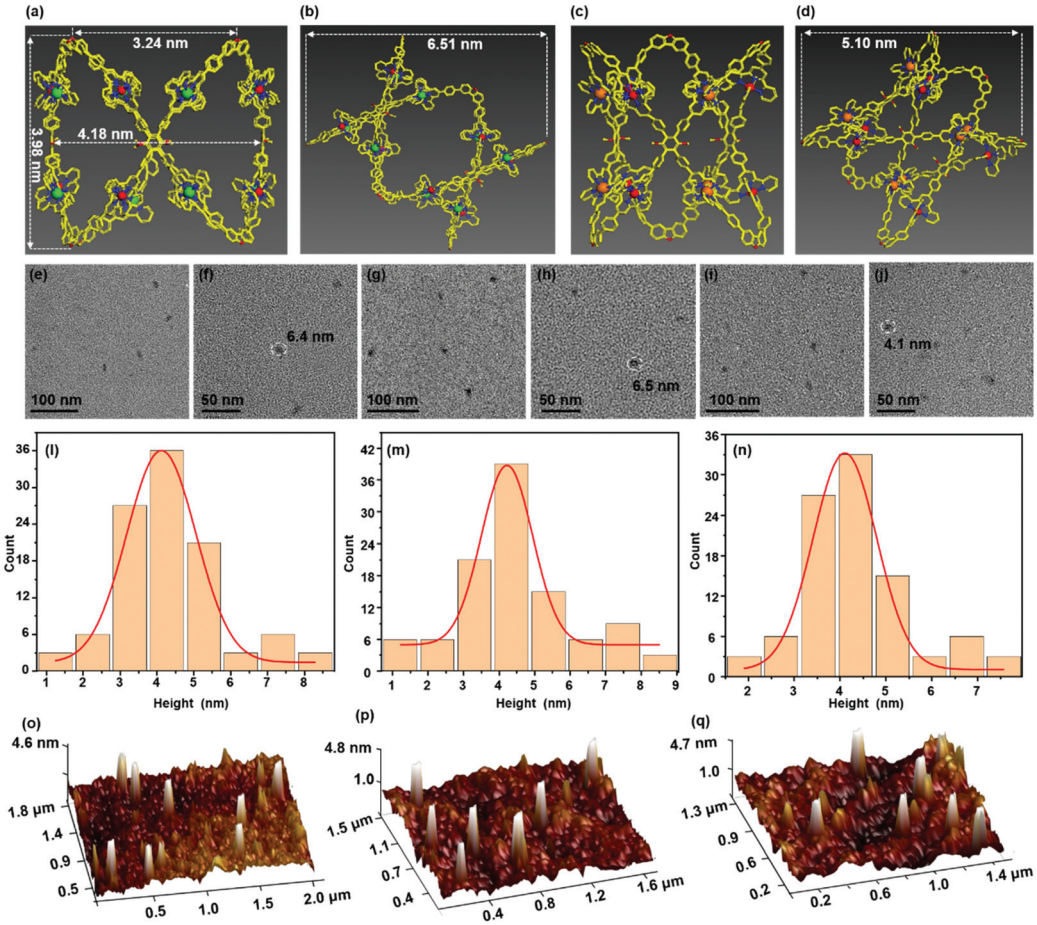

Fig. 4 (a) and (b) Representative energy-minimized structure of Co_8L_4 (Zn_8L_4), (c) and (d) representative energy-minimized structure of Cd_6L_3, (e) and (f) TEM images of Co_8L_4, (g) and (h) TEM images of Zn_8L_4, (i) and (j) TEM images of Cd_6L_3, (l)–(n) AFM height statistical histogram for 100 particles of Co_8L_4, Zn_8L_4, and Cd_6L_3, and (o)–(q) AFM images of Co_8L_4, Zn_8L_4 and Cd_6L_3.

platinum wire auxiliary electrode (CE), and an Ag/AgCl reference electrode (RE) with Bu_4NPF_6 (0.1 M) as the electrolyte. As can be observed from Fig. 5c, due to the reversible oxidation of Ru(III)/Ru(II) and Ru(IV)/Ru(III), the ligand **L** exhibits two oxidation peaks near 0.58 and 1.31 V.[34] As compared to ligand **L**, the oxidation peaks of the supramolecular structure demonstrate a slight positive shift. For [$\mathbf{Zn_8L_4}$] and [$\mathbf{Cd_6L_3}$], the oxidation peaks of Ru can be observed at 0.64 and 1.33 V, exhibiting a slight increment in the positive oxidation potential. Zn(II) and Cd(II) are difficult to oxidize under these conditions; thus, only Ru oxidation peaks can be observed for [$\mathbf{Zn_8L_4}$] and [$\mathbf{Cd_6L_3}$] (Fig. 5c and e).[35] For [$\mathbf{Co_8L_4}$], the oxidation peaks of Ru exhibit a similar slight positive shift (0.66 V, 1.32 V). Interestingly, the oxidation potential of Co(III)/Co(II) appears at 0.66 V in [$\mathbf{Co_8L_4}$], while the oxidation peak of the common Co-terpyridine complex is observed at 0.45 V (Fig. 5d).[24,36] The obvious positive shift indicates an effective improvement of oxidation ability which is anticipated to facilitate the oxygen evolution reactions.[37] The photophysical properties of these complexes were also investigated using UV-vis and low-temperature fluorescence spectroscopy. The absorption spectra of

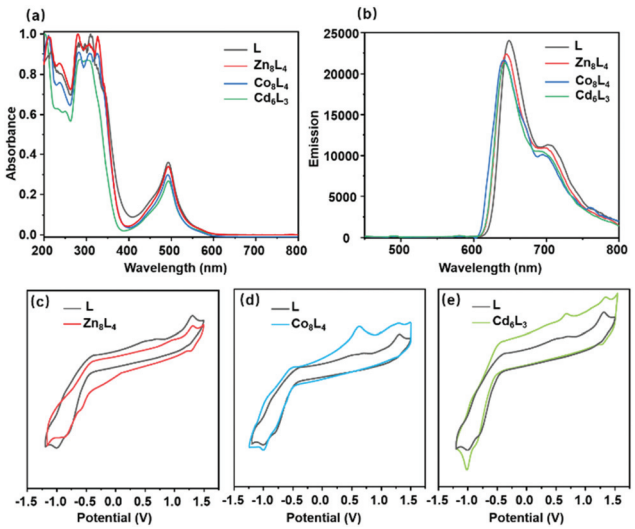

Fig. 5 UV–vis (a) (10^{-6} M in CH_3CN, room temperature) and emission (b) (10^{-6} M in CH_3CN, 73 K) of Zn_8L_4, Co_8L_4, and Cd_6L_3, CV of **L** with (c) Zn_8L_4, (d) Co_8L_4, and (e) Cd_6L_3 (in a 0.1 M solution of Bu_4NPF_6 in CH_3CN).

the ligands and all the complexes demonstrate a characteristic absorption peak near 485 nm (Fig. 5a), which can be attributed to the metal–ligand charge transfer transition of the tpy-Ru-tpy unit. The emission of **L** and supramolecules was examined in CH_3CN below 73 K (Fig. 5b). Compared with the ligand **L**, all supramolecules exhibit a slight decrease in the emission spectra and a minor shift, from 651 nm to 648 nm.[38]

Conclusion

Briefly, the tetra-terpyridine metal–organic ligand **L** with multi-axial coordination was designed and synthesized using a self-assembly-directed binding strategy. Subsequently, different three-dimensional metal–organic supramolecular structures were assembled based on the difference in the transition metal-binding ability. When **L** was combined with strongly binding metals (Zn and Co), tetrameric structures were formed. However, on combining with the weaker binding metal Cd, a trimeric structure was obtained. 1D and 2D NMR, ESI-MS, TWIM-MS, gMS^2, TEM, and AFM analyses were performed to characterize the molecular structure, size, and symmetry of the target assemblies. In addition, the photovoltaic properties of the supramolecular structures were also characterized by UV-vis, FL, and CV. The findings reported in this study are conducive to the comprehensive understanding of the effect of metal–ligand binding abilities on the supramolecular structures. As a result, these findings inspire us to obtain adaptive or stimuli-responsive materials, with potential applications in electrocatalytic oxygen precipitation, *etc*.

Author contributions

All authors have approved the final version of the manuscript. P. W. and Z. Z. designed the experiments; Q. B. completed the synthesis; T. W. and Y. L. carried out the NMR analysis; G. C. and Y. G. did the TEM tests; Q. B. and Z. Z. did the ESI-MS test and data curation; Y. L. and Q. B. analyzed the experiment data. M. W. and H. S. did the AFM tests; Q. B. wrote the manuscript. Z. Z., T. X., and P. W. edited the manuscript. All the authors discussed the results, and commented on and proofread the manuscript.

Conflicts of interest

There are no conflicts to declare.

Acknowledgements

This research was supported by the National Natural Science Foundation of China (21971257 to P. W., 22101061 to Z. Z., 21971048 for T.-Z. X.), the Guangdong Natural Science Foundation (2019A1515011358 to Z. Z.), the Science and Technology Research Project of Guangzhou (202002030257 to Z. Z.) and the Open Fund of Guangdong Provincial Key Laboratory of Functional Supramolecular Coordination Materials and Applications (2020A07 to Z. Z.). The authors thank for the TEM test and the assistance during data collection from the Modern Analysis and Testing Center of Guangzhou University. The authors would like to express their gratitude to EditSprings (https://www.editsprings.cn) for the expert linguistic services provided.

Notes and references

1 (*a*) G. R. Newkome and C. N. Moorefield, From 1 → 3 dendritic designs to fractal supramacromolecular constructs: understanding the pathway to the Sierpiński gasket, *Chem. Soc. Rev.*, 2015, **44**, 3954–3967; (*b*) Y. Sun, C. Chen, J. Liu and P. J. Stang, Recent developments in the construction and applications of platinum-based metallacycles and metallacages via coordination, *Chem. Soc. Rev.*, 2020, **49**, 3889–3919.

2 (*a*) Y. Jin, Y. Hu and W. Zhang, Tessellated multiporous two-dimensional covalent organic frameworks, *Nat. Rev. Chem.*, 2017, **1**, 0056–0066; (*b*) G.-Y. Wu, X. Shi, H. Phan, H. Qu, Y.-X. Hu, G.-Q. Yin, X.-L. Zhao, X. Li, L. Xu, Q. Yu and H.-B. Yang, Efficient self-assembly of heterometallic triangular necklace with strong antibacterial activity, *Nat. Commun.*, 2020, **11**, 3178–3188.

3 K. Ariga, H. Ito, J. P. Hill and H. Tsukube, Molecular recognition: from solution science to nano/materials technology, *Chem. Soc. Rev.*, 2012, **41**, 5800–5835.

4 L.-J. Chen, Y.-Y. Ren, N.-W. Wu, B. Sun, J.-Q. Ma, L. Zhang, H. Tan, M. Liu, X. Li and H.-B. Yang, Hierarchical self-assembly of discrete organoplatinum(II) metallacycles with polysaccharide via electrostatic interactions and their application for heparin detection, *J. Am. Chem. Soc.*, 2015, **137**, 11725–11735.

5 M. H. Lee, J. S. Kim and J. L. Sessler, Small molecule-based ratiometric fluorescence probes for cations, anions, and biomolecules, *Chem. Soc. Rev.*, 2015, **44**, 4185–4191.

6 (*a*) J. S. Mugridge, A. Zahl, R. van Eldik, R. G. Bergman and K. N. Raymond, Solvent and pressure effects on the motions of encapsulated guests: tuning the flexibility of a supramolecular host, *J. Am. Chem. Soc.*, 2013, **135**, 4299–4306; (*b*) M. Schulze, V. Kunz, P. D. Frischmann and F. Würthner, A supramolecular ruthenium macrocycle with high catalytic activity for water oxidation that mechanistically mimics photosystem II, *Nat. Chem.*, 2016, **8**, 576–583.

7 W. Wang, Y.-X. Wang and H.-B. Yang, Supramolecular transformations within discrete coordination-driven supramolecular architectures, *Chem. Soc. Rev.*, 2016, **45**, 2656–2693.

8 A. J. McConnell, C. S. Wood, P. P. Neelakandan and J. R. Nitschke, Stimuli-responsive metal-ligand assemblies, *Chem. Rev.*, 2015, **115**, 7729–7793.

9 A. M. Lifschitz, M. S. Rosen, C. M. McGuirk and C. A. Mirkin, Allosteric supramolecular coordination constructs, *J. Am. Chem. Soc.*, 2015, **137**, 7252–7261.

10 I. A. Riddell, Y. R. Hristova, J. K. Clegg, C. S. Wood, B. Breiner and J. R. Nitschke, Five discrete multinuclear metal-organic assemblies from one ligand: deciphering the effects of different templates, *J. Am. Chem. Soc.*, 2013, **135**, 2723–2733.

11 S. M. Jansze, G. Cecot, M. D. Wise, K. O. Zhurov, T. K. Ronson, A. M. Castilla, A. Finelli, P. Pattison, E. Solari, R. Scopelliti, G. E. Zelinskii, A. V. Vologzhanina, Y. Z. Voloshin, J. R. Nitschke and K. Severin, Ligand aspect ratio as a decisive factor for the self-assembly of coordination cages, *J. Am. Chem. Soc.*, 2016, **138**, 2046–2054.

12 (*a*) X. Lu, X. Li, K. Guo, T.-Z. Xie, C. N. Moorefield, C. Wesdemiotis and G. R. Newkome, Probing a hidden world of molecular self-assembly: concentration-dependent, three-dimensional supramolecular interconversions, *J. Am. Chem. Soc.*, 2014, **136**, 18149–18155; (*b*) T. Wu, Z. Jiang, X. Xue, S.-C. Wang, M. Chen, J. Wang, H. Liu, J. Yan, Y.-T. Chan and P. Wang, Molecular hexagram and octagram: Position determined 3D metallo-supermolecules and concentration-induced transformation, *Chin. Chem. Lett.*, 2021, **32**, 1911–1914.

13 T.-Z. Xie, K. Guo, Z. Guo, W.-Y. Gao, L. Wojtas, G.-H. Ning, M. Huang, X. Lu, J.-Y. Li, S.-Y. Liao, Y.-S. Chen, C. N. Moorefield, M. J. Saunders, S. Z. D. Cheng, C. Wesdemiotis and G. R. Newkome, Precise molecular fission and fusion: quantitative self-Assembly and chemistry of a metallo-cuboctahedron, *Angew. Chem., Int. Ed.*, 2015, **54**, 9224–9229.

14 (*a*) O. Gidron, M. Jirásek, N. Trapp, M.-O. Ebert, X. Zhang and F. Diederich, Homochiral [2]catenane and bis[2]catenane from alleno-acetylenic helicates - a highly selective narcissistic self-sorting process, *J. Am. Chem. Soc.*, 2015, **137**, 12502–12505; (*b*) B. Kilbas, S. Mirtschin, R. Scopelliti and K. Severin, A solvent-responsive coordination cage, *Chem. Sci.*, 2012, **3**, 701–704.

15 B. Li, W. Zhang, S. Lu, B. Zheng, D. Zhang, A. Li, X. Li, X.-J. Yang and B. Wu, Multiple transformations among anion-based $A_{2n}L_{3n}$ assemblies: bicapped trigonal antiprism A_8L_{12}, tetrahedron A_4L_6, and triple helicate A_2L_3 (A = Anion), *J. Am. Chem. Soc.*, 2020, **142**, 21160–21168.

16 K. Oji, A. Igashira-Kamiyama, N. Yoshinari and T. Konno, Formation, expansion, and interconversion of metallarings in a sulfur-bridged auICoIII coordination system, *Angew. Chem., Int. Ed.*, 2014, **53**, 1992–1996.

17 C. S. Pecinovsky, E. S. Hatakeyama and D. L. Gin, Polymerizable photochromic macrocyclic metallomesogens: design of supramolecular polymers with responsive nanopores, *Adv. Mater.*, 2008, **20**, 174–178.

18 (*a*) N. Kishi, M. Akita and M. Yoshizawa, Selective host–guest interactions of a transformable coordination capsule/tube with fullerenes, *Angew. Chem., Int. Ed.*, 2014, **53**, 3604–3607; (*b*) M. D. Ward, C. A. Hunter and N. H. Williams, Coordination cages based on bis(pyrazolylpyridine) ligands: structures, dynamic behavior, guest binding, and catalysis, *Acc. Chem. Res.*, 2018, **51**, 2073–2082.

19 S. J. Lee and W. Lin, Chiral metallocycles: rational synthesis and novel applications, *Acc. Chem. Res.*, 2008, **41**, 521–537.

20 F. Würthner, C.-C. You and C. R. Saha-Möller, Metallosupramolecular squares: from structure to function, *Chem. Soc. Rev.*, 2004, **33**, 133–146.

21 I. A. Riddell, T. K. Ronson, J. K. Clegg, C. S. Wood, R. A. Bilbeisi and J. R. Nitschke, Cation- and anion-exchanges induce multiple distinct rearrangements within metallosupramolecular architectures, *J. Am. Chem. Soc.*, 2014, **136**, 9491–9498.

22 (*a*) J. Wang, H. Zhao, M. Chen, Z. Jiang, F. Wang, G. Wang, K. Li, Z. Zhang, D. Liu, Z. Jiang and P. Wang, Construction of macromolecular pinwheels using predesigned metalloligands, *J. Am. Chem. Soc.*, 2020, **142**, 21691–21701; (*b*) T. Wu, Z. Jiang, Q. Bai, Y. Li, S. Mao, H. Yu, L. Wojtas, Z. Tang, M. Chen, Z. Zhang, T.-Z. Xie, M. Wang, X. Li and P. Wang, Supramolecular triangular orthobicupola: Self-assembly of a giant Johnson solid J_{27}, *Chem*, 2021, **7**, 2429–2441.

23 Z. Zhang, Y. Li, B. Song, Y. Zhang, X. Jiang, M. Wang, R. Tumbleson, C. Liu, P. Wang, X.-Q. Hao, T. Rojas, A. T. Ngo, J. L. Sessler, G. R. Newkome, S. W. Hla and X. Li, Intra- and intermolecular self-assembly of a 20 nm-wide supramolecular hexagonal grid, *Nat. Chem.*, 2020, **12**, 468–474.

24 L. Wang, B. Song, S. Khalife, Y. Li, L.-J. Ming, S. Bai, Y. Xu, H. Yu, M. Wang, H. Wang and X. Li, Introducing seven transition metal ions into terpyridine-based supramolecules: self-assembly and dynamic ligand exchange study, *J. Am. Chem. Soc.*, 2020, **142**, 1811–1821.

25 Q. Bai, T. Wu, Z. Zhang, L. Xu, Z. Tang, Y. Guan, T.-Z. Xie, M. Chen, P. Su, H. Wang, P. Wang and X. Li, Clover leaf-shaped supramolecules assembled using a predesigned metallo-organic ligand, *Org. Chem. Front.*, 2021, **8**, 3244–3249.

26 E. C. Constable, K. Harris, C. E. Housecroft, M. Neuburger and J. A. Zampese, Turning $\{M(tpy)2\}^{n+}$ embraces and CH···π interactions on and off in homoleptic cobalt(ii) and cobalt(iii) bis(2,2′:6′,2″-terpyridine) complexes, *CrystEngComm*, 2010, **12**, 2949–2961.

27 H. S. Chow, E. C. Constable, C. E. Housecroft, K. J. Kulicke and Y. Tao, When electron exchange is chemical exchange-assignment of ^{1}H NMR spectra of paramagnetic cobalt(ii)-2,2′:6′,2″-terpyridine complexes, *Dalton Trans.*, 2005, **2**, 236–237.

28 S. Perera, X. Li, M. Soler, A. Schultz, C. Wesdemiotis, C. N. Moorefield and G. R. Newkome, Hexameric palladium(II) terpyridyl metallomacrocycles: assembly with 4,4′-Bipyridine and characterization by TWIM mass spectrometry, *Angew. Chem., Int. Ed.*, 2010, **49**, 6539–6544.

29 M. A. R. Meier, B. G. G. Lohmeijer and U. S. Schubert, Relative binding strength of terpyridine model complexes under matrix-assisted laser desorption/ionization mass spectrometry conditions, *J. Mass Spectrom.*, 2003, **38**, 510–516.

30 X. Li, Y.-T. Chan, G. R. Newkome and C. Wesdemiotis, Gradient tandem mass spectrometry interfaced with ion

mobility separation for the characterization of supramolecular architectures, *Anal. Chem.*, 2011, **83**, 1284–1290.

31 M. Satterfield and J. S. Brodbelt, Relative binding energies of gas-phase pyridyl ligand/metal complexes by energy-variable collisionally activated dissociation in a quadrupole ion trap, *Inorg. Chem.*, 2001, **40**, 5393–5400.

32 T. Kraus, M. Buděšínský, J. Cvačka and J.-P. Sauvage, Copper(I)-directed formation of a cyclic pseudorotaxane tetramer and its trimeric homologue, *Angew. Chem., Int. Ed.*, 2006, **45**, 258–261.

33 (*a*) T. Ichijo, S. Sato and M. Fujita, Size-, mass-, and density-controlled preparation of TiO_2 banoparticles in a spherical cccoordination template, *J. Am. Chem. Soc.*, 2013, **135**, 6786–6789; (*b*) C. Wang, X.-Q. Hao, M. Wang, C. Guo, B. Xu, E. N. Tan, Y.-Y. Zhang, Y. Yu, Z.-Y. Li, H.-B. Yang, M.-P. Song and X. Li, Self-assembly of giant supramolecular cubes with terpyridine ligands as vertices and metals on edges, *Chem. Sci.*, 2014, **5**, 1221–1226.

34 (*a*) L. Duan, F. Bozoglian, S. Mandal, B. Stewart, T. Privalov, A. Llobet and L. Sun, A molecular ruthenium catalyst with water-oxidation activity comparable to that of photosystem II, *Nat. Chem.*, 2012, **4**, 418–423; (*b*) M. Schulze, V. Kunz, P. D. Frischmann and F. Würthner, A supramolecular ruthenium macrocycle with high catalytic activity for water oxidation that mechanistically mimics photosystem II, *Nat. Chem.*, 2016, **8**, 576–583.

35 Z. Zhang, H. Wang, X. Wang, Y. Li, B. Song, O. Bolarinwa, R. A. Reese, T. Zhang, X.-Q. Wang, J. Cai, B. Xu, M. Wang, C. Liu, H.-B. Yang and X. Li, Supersnowflakes: stepwise self-assembly and dynamic exchange of rhombus starshaped supramolecules, *J. Am. Chem. Soc.*, 2017, **139**, 8174–8185.

36 I. F. Mansoor, D. I. Wozniak, Y. Wu and M. C. Lipke, A delocalized cobaltoviologen with seven reversibly accessible redox states and highly tunable electrochromic behaviour, *Chem. Commun.*, 2020, **56**, 13864–13867.

37 Q. Liu, Q. Wang, J. Wang, Z. Li, J. Liu, X. Sun, J. Li, Y. Lei, L. Dai and P. Wang, $TpyCo_2^+$-based coordination polymers by water-induced gelling trigged efficient oxygen evolution reaction, *Adv. Funct. Mater.*, 2020, **30**, 2000593–2000599.

38 M. Galletta, S. Campagna, M. Quesada, G. Ulrich and R. Ziessel, The elusive phosphorescence of pyrromethene–BF_2 dyes revealed in new multicomponent species containing Ru(ii)–terpyridine subunits, *Chem. Commun.*, 2005, **33**, 4222–4224.

